SCIENCE CHINA
Chemistry

•ARTICLES•

https://doi.org/10.1007/s11426-020-9762-0

Pestaloamides A and B, two spiro-heterocyclic alkaloid epimers from the plant endophytic fungus *Pestalotiopsis* sp. HS30

Xiao-Zheng Su[1,2†], Yi-Ying Zhu[1†], Jian-Wei Tang[1], Kun Hu[1], Xiao-Nian Li[1], Han-Dong Sun[1], Yan Li[1*] & Pema-Tenzin Puno[1*]

[1]*State Key Laboratory of Phytochemistry and Plant Resources in West China, Kunming Institute of Botany, Chinese Academy of Sciences; Yunnan Key Laboratory of Natural Medicinal Chemistry, Kunming 650201, China ;*
[2]*University of Chinese Academy of Sciences, Beijing 100049, China*

Received March 28, 2020; accepted April 26, 2020; published online May 19, 2020

Pestaloamides A and B (**1** and **2**), two novel alkaloids featuring an unprecedented spiro[imidazothiazoledione-alkylidenecyclopentenone] scaffold, were obtained from the cultures of an endophytic fungus *Pestalotiopsis* sp. HS30 which inhabited the stems of *Isodon xerophilus*. Their planar structures and absolute configurations were fully determined by extensive spectroscopic analysis and X-ray crystallography. In addition, both compounds **1** and **2** showed the latent tumor immunotherapy activity through markedly promoting the cell surface engagement of NKG2D ligands involving MICA/B and ULBP1 in HCT116 cells.

alkaloids, endophytic fungus, structure elucidation, tumor immunotherapy

Citation: Su XZ, Zhu YY, Tang JW, Hu K, Li XN, Sun HD, Li Y, Puno PT. Pestaloamides A and B, two spiro-heterocyclic alkaloid epimers from the plant endophytic fungus *Pestalotiopsis* sp. HS30. *Sci China Chem*, 2020, 63, https://doi.org/10.1007/s11426-020-9762-0

1 Introduction

Cancer immunotherapy, which strengthens the congenital immune systems to recognize and obliterate malignant cells with minimum effect to normal tissue and continuous memory for prevention of tumor relapse, has showed prospective clinical cancer treatment over past few years [1]. As a component of the innate immunological system, natural killer (NK) cells play a significant role in tumorous clearance [2]. The activity of NK cells is mainly controlled through the interactions between its receptors such as NK grout 2 member D (NKG2D) and ligands of tumor cells, which reveals that NKG2D ligands may become a crucial target about antitumor immunization [3]. The natural product, such as, phomoxanthone A, a secondary metabolite from the endophytic fungus *Phomopsis longicolla*, was reported to be a potent activator of NK cells for eradication tumor cells [4]. Besides, our recent study, parvifoline AA, from the plants of genus *Isodon*, suggested mediating NK cells associated immune surveillance by manipulating expression of NKG2D ligands in hepatocellular carcinoma (HCC) cells [5].

As a very important part of discovering more structurally novel leads with antitumor immune activity, we have screened the endophytic fungi of the *Isodon* species by using our previous reported screening strategy [6]. The screening led us to discover a promising strain which colonized in the stems of *Isodon xerophilus* named *Pestalotiopsis* sp. HS30. Specifically, the abundant peaks in its high performance liquid chromatography (HPLC) profile and very interesting nodes in its molecular networking (Figures S1–S2, Supporting Information online) made it stick out from the other candidates. Subsequently, we performed large fermentation of this strain and conducted a deeper exploration about its secondary metabolites which led to the discovery of pesta-

†These authors contributed equally to this work.
*Corresponding authors (email: liyanb@mail.kib.ac.cn; punopematenzin@mail.kib.ac.cn)

loamides A and B (**1** and **2**) (Figure 1), two novel alkaloids possessing an unprecedented spiro[imidazothiazoledione-alkylidenecyclopentenone] skeleton. Furthermore, compounds **1** and **2** obviously upregulated expression of NKG2D ligands on the surface of human colorectal cancer cell line HCT116 to exhibit potential antitumor immune response, while compound **2** showed better ligands restoring activity than **1**. Herein, we describe the isolation, structure elucidation, and plausible biogenetic pathways as well as bioactivity evaluation of compounds **1** and **2**.

2 Experimental

General procedure. Optical rotations were measured with a JASCO P-1020 polarimeter (Japan). UV spectra were obtained using a Shimadzu UV-2401 PC spectrophotometer (Japan). A Tensor 27 spectrophotometer was used for scanning IR spectroscopy with KBr pellets (Bruker, Germany). 1D and 2D nuclear magnetic resonance (NMR) spectra were recorded on Bruker DRX-800 spectrometers with TMS as internal standard. Chemical shifts (δ) are expressed in parts per million (ppm) with reference to the solvent signals. High resolution electrospray ionization mass spectroscopy (HRESIMS) was performed on an API QSTAR spectrometer. Semipreparative HPLC was performed on an Agilent 1200 liquid chromatograph (USA) with a Zorbax SB-C18 (9.4 mm×250 mm) column. Liquid chromatography-tandem mass spectrometry (LC-MS/MS) was performed on Agilent 6530 Accurate-Mass Q-TOF spectrometer coupled to an Agilent 1290 LC system with Zorbax SB-C18 (9.4 mm×250 mm) column. Column chromatography was performed with silica gel (100–200 mesh, Qingdao Marine Chemical, Inc., China). Fractions were monitored by thin layer chromatography (TLC), and spots were visualized by heating silica gel plates sprayed with 10% H_2SO_4 in EtOH.

Fungal material, identification and fermentation. The fungal strain of *Pestalotiopsis* sp. HS30 was isolated from fresh stems of *Isodon xerophilus* that was collected from Kunming Botanical Garden, Kunming City, Yunnan Province, China, in August 2018. The isolate was identified based on sequence (GenBank Accession No. MT211378) analysis of the ITS region of the rDNA. The fungal strain was cultured on slants of potato dextrose agar at 28 °C for 7 d. Agar plugs were cut into small pieces (about 0.5 cm×0.5 cm×0.5 cm) under aseptic condition, and 15 pieces were used to inoculate three Erlenmeyer flasks (500 mL), each containing 200 mL of media (0.4% glucose, 1% malt extract, and 0.4% yeast extract); the final pH of the media was adjusted to 7.0, and flasks were sterilized by autoclave. Three flasks of the inoculated media were incubated at 28 °C on a rotary shaker at 170 r min^{-1} for 7 d to prepare the seed culture. Spore inoculum was prepared in sterile, distilled H_2O to give a final spore/cell suspension of 1×10^6 mL^{-1} which was calculated by using hemocytometer. The detailed larger fermentation procedure was as following: fermentation was carried out on solid rice medium in 65 Fernbach flasks (500 mL, 90 mL distilled water was added to 80 g rice and kept overnight before autoclaving). Each flask was inoculated with 5.0 mL of the spore inoculum and incubated for 30 d at 28 °C in a static incubator.

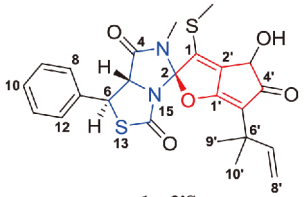

Figure 1 Structures of pestaloamides A and B (**1** and **2**) (color online).

Extraction and isolation. The medium was overlaid and extracted with MeOH by maceration. With filtration and concentration, the resultant extract was partitioned with EtOAc. Then the solvent was evaporated *in vacuo* to afford a crude extract (45 g). The extraction was subjected to column chromatography on silica gel with a $CHCl_3/Me_2CO$ gradient system (1:0, 9:1, 8:2, 7:3, 6:4, 1:1, 0:1) to yield seven fractions, A–G. Fraction B ($CHCl_3/Me_2CO$, 9:1, 12 g) was chromatographed on a RP-18 column with a methanol/H_2O gradient system (from 10:90 to 100:0) to afford fractions B1–B10. Fraction B7 (methanol/H_2O, 70:30, 602 mg) was subjected to chromatography over silica gel (petroleum ether/Me_2CO, from 80:1 to 0:1) to yield subfractions B7/1-16, subfraction B7-10 was purified by semipreparative HPLC (3 mL/min, detector UV λ_{max}=195 nm, MeCN/H_2O, 51:49) to yield **1** (2 mg, retention time=42 min), and subfraction B7-9 was purified by semipreparative HPLC (3 mL min^{-1}, detector UV λ_{max}=195 nm, MeCN/H_2O, 50:50) to yield **2** (1.8 mg, retention time=39 min).

X-ray crystal structure analysis. The intensity data for pestaloamides A and B (**1** and **2**) were collected on a Bruker APEX DUO diffractometer (Germany) using graphite-monochromated Cu Kα radiation. The structures of these compounds were solved by direct methods (SHELXS97), expanded using difference Fourier techniques, and refined by the program and full-matrix least-squares calculations. The non-hydrogen atoms were refined anisotropically, and hydrogen atoms were fixed at calculated positions. Detailed data were provided in Tables S1–S16 in the Supporting Information online.

Antitumor immune bioassays. Human colorectal cancer cell line HCT116 was obtained from Shanghai Institute of Biochemistry and Cell Biology, Chinese Academy of Sciences (China). HCT116 cells were cultured in RPMI-1640 (Biological Industries) supplemented with 10% fetal bovine

serum (Biological Industries) and 1% penicillin and 1% streptomycin. Cells were cultured at 37 °C in a humidified atmosphere with 5% CO_2. The murine anti-human MICA/B-APC, ULBP1-APC, ULBP2-APC, ULBP3-APC and IgG-APC were purchased from R&D system (USA). The flow cytometry analysis was performed as previously reported [5,7]. Briefly, collected cells were stained with indicated APC-conjugated Abs or IgG followed by being washed and suspended in phosphate buffer saline (PBS). Samples were examined on a FACS Calibur flow cytometer (BD Bioscience, USA). And data were analyzed using FlowJo10.3 analysis software.

*Physical constants and spectroscopic data of compounds **1** and **2***. Pestaloamide A (**1**): initially obtained as a white amorphous powder, by using slow evaporation of methanol in a closed tube, the crystal was obtained eventually; m.p.: 130–135 °C; [α]23 D: −27.90 (MeOH, *c*, 0.060); ECD (MeOH) λ_{max} (log ε): 208 (0.67), 239 (0.12), 257 (−0.39), 299 (0.52), and 335 (−0.37) nm; UV (MeOH) λ_{max} (log ε): 195 (4.45), 269 (3.55), and 309 (4.11) nm; IR (ν_{max}): 3,428, 2,962, 2,872, 1,707, 1,617, 1,499, 1,384, 741, and 697 cm^{-1}. HRESIMS at *m*/*z* 485.1195 ($[M+H]^+$, calcd. for 485.1199. ^1H and ^{13}C NMR data, see Table 1.

Pestaloamide B (**2**): isolated as yellow needle crystals by using vapor exchange method of methanol and water in a closed glass tube; m.p.: 138–140 °C; [α]19.3 D: +101.17 (MeOH, *c*, 0.070); ECD (MeOH) λ_{max} (log ε): 205 (0.67), 244 (0.12), 262 (–0.39), 269 (0.52), 295 (–0.37), and 332 (1.28) nm; UV (MeOH) λ_{max} (log ε): 195 (4.66), 269 (3.77), and 308 (4.22) nm; IR (ν_{max}): 3,428, 2,962, 2,872, 1,707, 1,617, 1,499, 1,384, 741, and 697 cm^{-1}. HRESIMS at *m*/*z* 507.1023 ($[M+Na]^+$, calcd. for 507.1019. ^1H and ^{13}C NMR data, see Table 1.

Crystallographic data for the structures of pestaloamide A (**1**, deposition number CCDC 1990908) and pestaloamide B (**2**, deposition number CCDC 1990909) have been deposited in the Cambridge Crystallographic Data Centre database. Copies of the data can be obtained free of charge from the CCDC at www.ccdc.cam.ac.uk.

Crystal data for **1**: $C_{24}H_{24}N_2O_5S_2{\bullet}H_2O$, *M*=502.59, *a*=9.8540(3) Å, *b*=6.6593(2) Å, *c*=17.9125(5) Å, α=90°, β=92.5420(10)°, γ=90°, *V*=1174.27(6) $Å^3$, *T*=100.(2) K, space group *P*1211, *Z*=2, μ(Cu Kα)=2.433 mm^{-1}, 24,524 reflections measured, 4,470 independent reflections (R_{int} =0.0543). The final R_1 values were 0.0571 ($I>2\sigma(I)$). The final $wR(F^2)$ values were 0.1569 ($I>2\sigma(I)$). The final R_1 values were 0.0637 (all data). The final $wR(F^2)$ values were 0.1646 (all data). The goodness of fit on F^2 was 1.063. Flack

Table 1 ^1H NMR (800 MHz), ^{13}C NMR (200 MHz) and HMBC data of **1** and **2** (δ (ppm), *J* (Hz)) recorded in CD_3OD

No.	**1**		**2**		HMBC
	δ_H, mult. (*J*)	δ_C, type	δ_H, mult. (*J*)	δ_C, type	
1		131.5 C		131.2 C	
1-SCH_3	2.83 (s)	15.5 CH_3	2.79 (s)	15.0 CH_3	1
2		116.4 C		116.6 C	
3-NCH_3	2.74 (s)	25.1 CH_3	2.76 (s)	25.1 CH_3	2, 4
4		168.0 C		168.0 C	
5	5.28 (d, 11.5)	67.3 CH	5.26 (d, 11.5)	67.3 CH	4, 6, 7
6	5.41 (d, 11.5)	55.5 CH	5.42 (d, 11.5)	55.5 CH	4, 5, 7, 8, 12
7		135.3 C		135.3 C	
8/12	7.64 (d, 7.3)	129.9 CH	7.64 (d, 7.3)	129.9 CH	6, 9, 10, 11
9/11	7.43 (t, 7.4)	130.3 CH	7.43 (t, 7.4)	130.3 CH	7, 10
10	7.40 (m)	130.4 CH	7.39 (m)	130.4 CH	8, 12
14		170.1 C		170.3 C	
1′		178.8 C		178.9 C	
2′		136.8 C		136.8 C	
3′	4.72 (s)	69.6 CH	4.71 (s)	69.2 CH	1, 1′, 2′, 4′
4′		204.6 C		204.4 C	
5′		117.9 C		117.9 C	
6′		38.7 C		38.7 C	
7′	6.10 (dd, 17.4, 10.6)	146.2 CH	6.09 (dd, 17.4, 10.6)	146.2 CH	5′, 6′, 9′, 10′
8′	b 4.98 (dd, 17.4, 1.0) a 4.92 (dd, 10.6, 1.0)	111.6 CH_2	b 4.97 (dd, 17.4, 1.0) a 4.92 (dd, 10.6, 1.0)	111.6 CH_2	6′, 7′
9′	1.38 (overlap)	26.8 CH_3	1.38 (overlap)	26.8 CH_3	5′, 6′, 7′, 8′, 10′
10′	1.38 (overlap)	26.7 CH_3	1.38 (overlap)	26.7 CH_3	5′, 6′, 7′, 8′, 9′

parameter=0.045(11).

Crystal data for **2**: $C_{24}H_{24}N_2O_5S_2$, M=484.57, a=9.9655(3) Å, b=6.5441(2) Å, c=18.1070(5) Å, α=90°, β=91.2900(10)°, γ=90°, V=1180.55(6) Å^3, T=100.(2) K, space group $P1211$, Z=2, μ(Cu Kα)=2.368 mm^{-1}, 25,017 reflections measured, 4,594 independent reflections (R_{int}=0.0683). The final R_1 values were 0.0653 ($I>2\sigma(I)$). The final $wR(F^2)$ values were 0.1759 ($I>2\sigma(I)$). The final R_1 values were 0.0705 (all data). The final $wR(F^2)$ values were 0.1832 (all data). The goodness of fit on F^2 was 1.041. Flack parameter=0.051(11).

3 Results and discussion

Pestaloamide A (**1**) was isolated as a powder initially and finally obtained as fine crystal in methanol solution. The molecular formula of **1** was determined as $C_{24}H_{24}N_2O_5S_2$ with the positive HRESIMS ion peak at m/z 485.1195 ([M+H]$^+$, calcd. for 485.1199), implying 14 degrees of unsaturation. Its IR spectrum suggested the presence of hydroxyl (3,428 cm^{-1}), methyl (2,962, 2,872 and 1,384 cm^{-1}), amide (1,707 cm^{-1}) and mono-substituted phenyl (1,671, 1,499, 741 and 697 cm^{-1}) groups. The ^{1}H NMR data (Table 1) gave two unusual methyl signals at δ_H 2.74 (s) and 2.83 (s), which insinuated that these methyls might be bonded to N or S heteroatoms. The analysis of its heteronuclear single quantum coherence (HSQC) and distortionless enhancement by polarization transfer (DEPT) spectra showed that the 24 carbon resonances were described as four methyls, one terminal olefinic methylene, nine methines (including five aromatics and one olefinic carbon), and ten non-protonated carbons (Table 1).

More details about the structure of **1** were provided by its 2D NMR spectra (Figures S7–S11). The protons at δ_H 7.40 (1H, m), 7.43 (2H, t, J=7.4 Hz), 7.64 (2H, d, J=7.3 Hz) and ^{1}H-^{1}H correlation spectroscopy (^{1}H-^{1}H COSY) of H-8(12)/H-9(11)/H-10 constituted the 1-substituted phenyl moiety. Moreover, the ^{1}H-^{1}H COSY correlation of H-5/H-6 with key heteronuclear multiple bond correlations (HMBCs) from H-9/11 to C-7 (δ_C, 135.3), from H-8/12 to C-6 (δ_C, 55.5), from H-6 to C-7 and C-4 (δ_C, 168.0), from H-5 to C-7 and C-4, and from H_3-3-NCH_3 (δ_H, 2.74) to C-4 and C-2 (δ_C, 116.4) assigned the mono-substituted phenyl as part of fragment A (Figure 2). The ^{1}H NMR spectrum signals of 6.10 (1H, dd, J=17.4, 10.6), 4.98 (1H, dd, J=17.4, 1.0), 4.92 (1H, dd, J=10.6, 1.0) and 1.38 (6H, overlap) and the ^{1}H-^{1}H COSY correlation of H-7′/H-8′ showed the existence of a prenyl moiety, which would be further confirmed by the HMBC correlations of H-8′ to C-6′ (δ_C, 38.7), H-7′ to C-6′ and C-5′ (δ_C, 117.9), and H3-9′ to C-5′, C-6′ and C-10′ (δ_C, 26.7). Therefore, on the basis of the ^{13}C NMR signals and the key HMBC correlations from H-3′ to C-1 (δ_C, 131.5), C-1′ (δ_C, 178.8), C-2′ (δ_C, 136.8) and C-4′ (δ_C, 204.6), and from H_3-1-SCH_3 (δ_H, 2.83) to C-1, the structure of fragment B (Figure 2) was finally determined. While the linkage among fragment A and B was difficult to establish with these data due to the consecutive of heteroatoms and non-protonated carbons. Fortunately, reliable evidence supporting the spiro[furan-2,5′-imidazo] skeleton of **1** was collected by acquiring the key LR-HSQMBC correlations from H_3-1-SCH_3/H-3′ to C-2, and from H-5 to C-1 combined with the characteristic chemical shift of C-2 (δ_C, 116.4) that was similar to Cyanogramide [8]. In consideration of the remined ^{13}C NMR signal of C-6 (δ_C, 55.5), residual hydrogen deficiency and the molecular formula, the structure and connection of fragment C (Figure 2) was deduced. Hereto, the planar structure of **1** was depicted as possessing a novel spiro[imidazothiazole-dione-alkylidenecyclopentenone] frame.

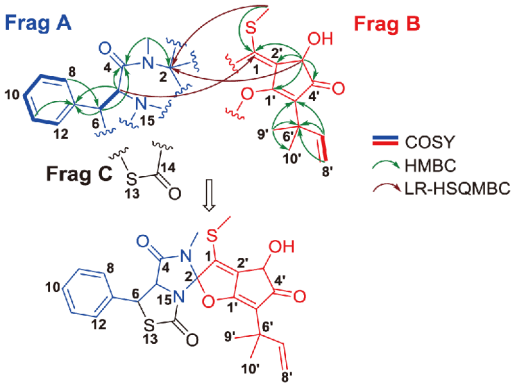

Figure 2 ^{1}H-^{1}H COSY, selected HMBC, and key LR-HSQMBC correlations of **1** and **2** (color online).

The coupling constant of H-5 and H-6 is 11.5 Hz which indicated the trans-relationship between H-5 and H-6 in an AB spin-spin coupled system. To explore the relative configuration of other position in compound **1**, the ROESY experiment was conducted. However, the correlations between H-6/H-8(12), H-5/H-8(12), H-3′/H_3-1-SCH_3, H-3′/H_3-3-NCH_3, H_3-9′(10′)/H-7′ and H_3-9′(10′)/H-8′ were unavailable for defining the relative configurations of C-2 and C-3′ (Figure 3). Luckily, suitable crystals of **1** were eventually obtained by slow evaporation of methanol. Then a single-crystal X-ray diffraction experiment with Cu Kα radiation of **1** (Flack parameter=0.045(11)) was performed (CCDC number: 1990908), which was consistent with above spectroscopic data not only confirmed the planar structure and relative configuration of **1** but also unambiguously revealed the absolute configuration as 2*R*, 5*S*, 6*S*, 3′*S* (Figure 4).

Pestaloamide B (**2**) obtained as yellow needle crystal with same molecular formula as **1** according to its HRESIMS (m/z 507.1023 [M+Na]$^+$, calcd. for 507.1019), which also indicated 14 indices of hydrogen deficiency. Comparison of 1D and 2D NMR spectra of **1** and **2**, a very similar pattern in both spectra except the weak shielded resonance of C-1-SCH_3 ($\Delta\delta_C$, −0.5) and C-3′ ($\Delta\delta_C$, −0.4) was shown in the ^{13}C

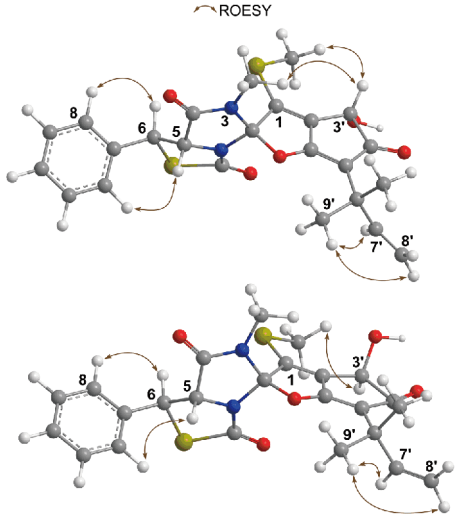

Figure 3 ROESY correlations of **1** and **2** (color online).

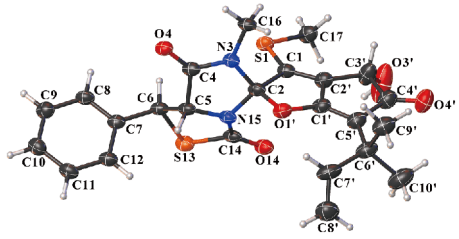

Figure 4 X-ray crystallographic structure of pestaloamide A (**1**) (color online).

NMR data of **2** (Table 1), which suggested that **2** might possess the same planar structure as **1** but different in relative configuration at position C-3′. Further evidence like unobserved ROESY correlation between H-3′/H_3-3-NCH_3 in **2** confirmed that compound **2** indeed was the C-3′ epimer of **1** with a 3′*R* configuration. Surprisingly, compound **2** was crystallized with vapor exchange method of MeOH/H_2O in a closed glass tube after repeated attempts. The absolute configuration of **2** was assigned as 2*R*, 5*S*, 6*S* and 3′*R* (Figure 5) by X-ray diffraction (Cu Kα) of the signal crystal in a Flack parameter of 0.051(11) (CCDC number: 1990909), which was consistent with aforementioned inference.

The intriguing structures, to some extent, implied a very unique biosynthetic pathway. The speculative biosynthesis pathways of **1** and **2** are illustrated in Scheme 1. The dipeptide Phe-Cys formed by L-phenylalanine and L-cystine generated an amide intermediate **i** with decarboxylation, dehydrogenation, and *N*,*S*-methylation. Then an intermolecular aldol condensation between oxidation product of **i** and a polyketide chain yielded **ii**. Dehydration and allylic oxidation of **ii** underwent an intramolecular aldol condensation to produce the cyclopentanone derivative **iv**. The decarboxylated and dehydrogenated **iv** was connected to an isopentenyl moiety by a prenyltransferase whose mechanism might be very similar to AnaPT, a prenyltransferase in acetylaszonalenin biosynthesis [9]. On account of intramolecular condensation, cyclization and dehydration, the formative **v** produced a key spiro[furan-2,5′-imidazo] derivative **vi**. Whereas the current knowledge about Sulphur insertion into secondary metabolites is quite limited. Therefore, we assumed that the precursor **viii** might be derived from carboxylation and hydroxylation of **vi** followed

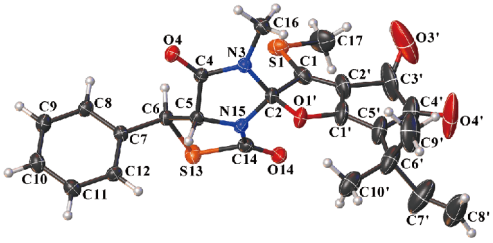

Figure 5 X-ray crystal structure of pestaloamide B (**2**) (color online).

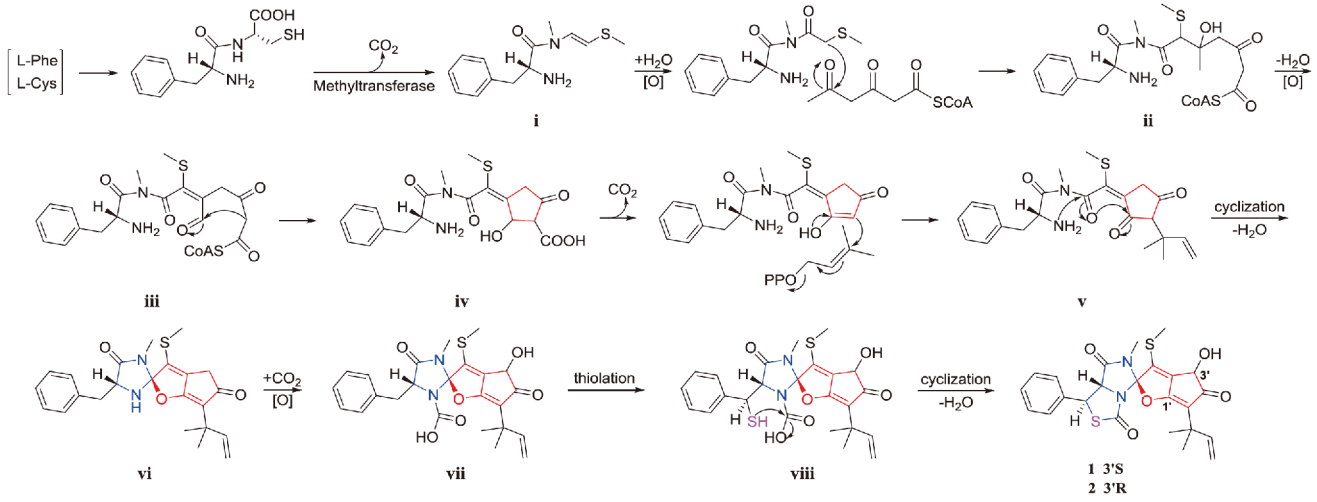

Scheme 1 Plausible biosynthetic pathways of **1** and **2** (color online).

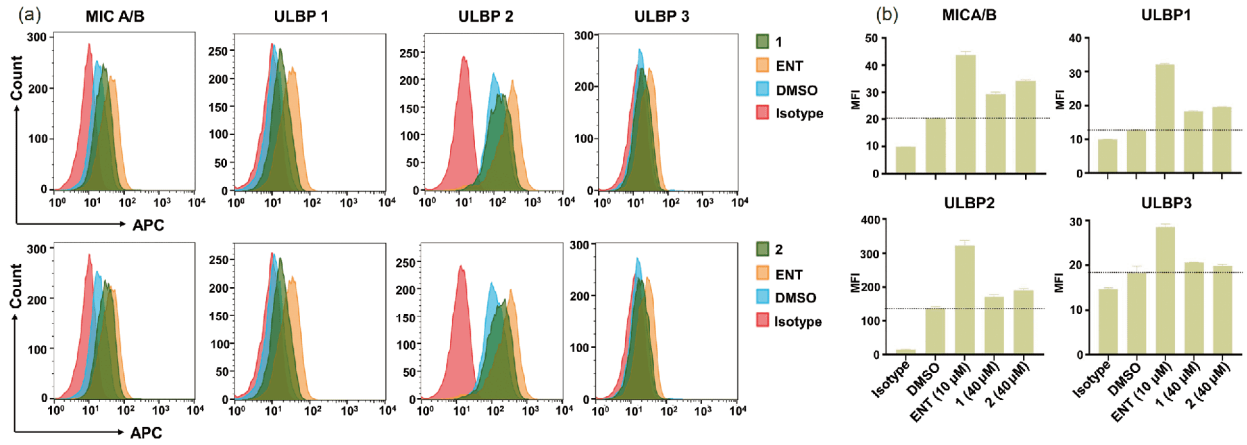

Figure 6 (a) HCT116 cells were treated with indicated compounds or vehicle for 24 h, and then the cell surface expression of MICA/B, ULBP1, ULBP2, and ULBP3 was detected by flow cytometry. DMSO served as negative control, and ENT served as positive control. (b) The mean fluorescence intensity of NKG2D ligands was presented as the histogram. The results were presented by the means of duplicate experiments±SD (color online).

by unique mechanism of C–S bond formation like biosynthesis of biotin [10]. Finally, the thioesterification of **viii** caused the production of compounds **1** and **2**.

NKG2D ligands in humans involve major histocompatibility complex (MHC) I-related chains A and B (MICA/B) and UL16-binding proteins (ULBPs) 1–6, which are associated with malignant transformation and tumorigenesis [11]. Binding of cell-bound ligands to the NKG2D receptor initiates the innate immune surveillance and tumor clearance in the early stage of tumorigenesis [12]. Generally, the NKG2D ligands are rarely detectable in normal cells but ubiquitously expressed in transformed cells, but cancer immune editing mechanism facilitates the immune evasion by reduction of NKG2D ligands density on the tumor cell surface in the progression of cancer, which leads to impaired activation of antitumor immune response [13]. Therefore, it is a promising and applicable strategy to increase the NKG2D ligands density on the tumor cell surface to efficiently activate antitumor immune response.

Flow cytometric analysis was performed to assess the effects of compounds **1** and **2** on the surficial engagement of NKG2D ligands including MICA/B and ULBPs on colorectal cancer HCT116 cells. As shown in Figure 6, the positive control entinostat (ENT) increased all the expression of cell surface ligands detected, while both **1** and **2** markedly enhanced the cell surface density of MICA/B, as well as ULBP1 and a slight upregulation of ULBP2 by compound **2**. Furthermore, a much stronger ligands engagement activity was observed in compound **2** treated cells compared with **1**, indicating the only configuration inversion of C-3′ might lead to discrepant activity of the promoted expression of NKG2D ligands between **1** and **2**. These data suggested compounds **1** and **2** could enhance the cell surface engagement of NKG2D ligands in HCT116 cells at a concentration of 40 μM, and the following antitumor immune responses and mechanism studies needed further researches.

Acknowledgements This work was supported by the Second Tibetan Plateau Scientific Expedition and Research (STEP) Program (2019QZKK0502), the National Natural Science Foundation of China (81874298), the CAS "Light of West China" Program (Pema-Tenzin Puno) and the Yunnan Science Fund for Distinguished Young Scholars (2019FJ002).

Conflict of interest The authors declare that they have no conflict of interest.

Supporting information The supporting information is available online at http://chem.scichina.com and http://link.springer.com/journal/11426. The supporting materials are published as submitted, without typesetting or editing. The responsibility for scientific accuracy and content remains entirely with the authors.

1 (a) Guo W, Liu L, Xiang C, Chen J, Liang XJ. *Sci China Chem*, 2019, 62: 1557–1560; (b) Ribas A, Wolchok JD. *Science*, 2018, 359: 1350–1355
2 Orange JS, Fassett MS, Koopman LA, Boyson JE, Strominger JL. *Nat Immunol*, 2002, 3: 1006–1012
3 Cifaldi L, Locatelli F, Marasco E, Moretta L, Pistoia V. *Trends Mol Med*, 2017, 23: 1156–1175
4 Rönsberg D, Debbab A, Mándi A, Vasylyeva V, Böhler P, Stork B, Engelke L, Hamacher A, Sawadogo R, Diederich M, Wray V, Lin WH, Kassack MU, Janiak C, Scheu S, Wesselborg S, Kurtán T, Aly AH, Proksch P. *J Org Chem*, 2013, 78: 12409–12425
5 Zhu H, Wang B, Kong L, An T, Li G, Zhou H, Gong L, Zhao Z, Gong Y, Sun H, Puno P, Li Y. *Cell Chem Biol*, 2019, 26: 1122–1132.e6
6 Tang JW, Kong LM, Zu WY, Hu K, Li XN, Yan BC, Wang WG, Sun HD, Li Y, Puno PT. *Org Lett*, 2019, 21: 771–775
7 Wu L, Wang S, Song Y, Wang X, Yan X. *Sci China Chem*, 2016, 59: 30–39
8 Fu P, Kong F, Li X, Wang Y, Zhu W. *Org Lett*, 2014, 16: 3708–3711
9 Yin WB, Grundmann A, Cheng J, Li SM. *J Biol Chem*, 2009, 284: 100–109
10 Fontecave M, Ollagnier-de-Choudens S, Mulliez E. *Chem Rev*, 2003, 103: 2149–2166
11 Li C, Ge B, Nicotra M, Stern JNH, Kopcow HD, Chen X, Strominger JL. *Proc Natl Acad Sci USA*, 2008, 105: 3017–3022
12 (a) Bae DS, Hwang YK, Lee JK. *Cell Immunol*, 2012, 276: 122–127; (b) Smyth MJ, Swann J, Cretney E, Zerafa N, Yokoyama WM, Hayakawa Y. *J Exp Med*, 2005, 202: 583–588
13 Nausch N, Cerwenka A. *Oncogene*, 2008, 27: 5944–5958